Deformation-Induced Martensitic Transformation Behavior of Retained Austenite during Rolling Contact

K. KANETANI T. MORONAGA T. HARA K. USHIODA

The deformation-induced martensitic transformation is a phenomenon that significantly improves the mechanical properties of steels, and is well known to be beneficial for the rolling contact fatigue (RCF) of bearings. In the present study, the characteristics of the deformation-induced martensitic transformation in the RCF of carburized, quenched and tempered SAE4320 steel were investigated in detail using scanning electron microscopy with electron backscattering diffraction and transmission electron microscopy with automated crystal orientation mapping. These analyses clarified that different variants of the extremely fine deformation-induced martensites as small as several tens of nm were formed within an austenite grain with RCF, and the martensites were speculated to have the Kurdjumov-Sachs or the Nishiyama-Wasserman relationship with the retained austenite. Furthermore, the deformation-induced martensites were preferentially formed within the retained austenite grains rather than at the interface between the tempered martensite and retained austenite. This suggests that the deformation-induced martensites were formed from some localized regions that were plastically introduced within the retained austenite grains.

***Key Words**: Rolling contact fatigue (RCF), Steel, Martensite, Austenite, Deformation-induced martensitic transformation, SEM, EBSD, ACOM, TEM*

1. Introduction

The deformation-induced transformation from austenite (γ) into martensite (α') while deforming steels containing metastable austenite, is well known. The deformation-induced martensitic transformation demonstrates a high level of plasticity and occurs when deforming austenite at a temperature of M_S or higher. In addition to the chemical composition of austenite, such as the amount of carbon in solid solution, the M_S temperature, stacking fault energy[1-7] and microstructural factors such as grain size[7-11], morphology[12-14] and crystal orientation[15, 16] of austenite, the transformation behavior is also heavily dependent on the stress state[17] and deformation temperature[18-20]. The transformation mechanism varies but is mainly dependent on the deformation temperature. As the temperature exceeds M_S, stress-induced martensitic transformation occurs during the elastic deformation of austenite in a similar manner as found in thermally induced regular martensite. Additionally, since the mechanical driving force required for martensitic transformation increases with temperature, austenite initially displays plastic deformation at temperatures above M_S^{σ} (temperature where the stress at which martensitic transformation starts and the stress where austenite yields are equal). The resulting local heterogeneous deformation areas (e.g. slip bands, shear bands, and deformation twins) and their intersecting areas result in strain-induced martensitic transformation[21]. Debate about the mechanisms of the martensitic transformation in the plastic deformation regime is ongoing[22]; however, several theories propose that martensitic transformation occurs due to the concentration of stresses in the intersection areas of deformation twins[23] and slip bands[24, 25] introduced by plastic deformation. Regardless of their formation mechanism, deformation-induced martensites significantly improve the mechanical properties of steel. TRIP (transformation-induced plasticity) steel, which has better balances between strength and ductility, makes use of this phenomenon. Since the proposal of high alloy TRIP steels by Zackay *et al.*[26] in the 1960s, the field has seen a wide range of developments, including that of low alloy TRIP steels for practical applications. Previous studies regarding the microstructural characteristics of deformation-induced martensite focus on single-phase austenitic high alloy TRIP steels. For instance, studies using Fe-Ni alloys[19, 20] showed that deformation-induced martensite subjected to tensile deformation above the M_S temperature is typical lenticular martensite with a mid-

**1 This paper is reprinted from ISIJ International, Vol. 61 (2021), No. 10, pp. 2629-2635 a part thereof is modified.*

rib. However, in contrast to the deformation mechanism of athermal martensite, deformation-induced martensite subjected to tensile deformation at higher temperatures has no mid-rib or deformation twins but instead forms notably fine butterfly martensite. Additionally, deforming Fe-Cr-Ni alloys with low stacking fault energy or austenitic stainless steels results first in hcp ε martensite, followed by the generation of bcc α' martensite from the ε phase[19, 27, 28] or α' martensite from slip bands[24, 25]. A study focusing on an Fe-Ni-Co-Ti alloy[29] reports that deformation-induced martensite will grow from thin plate martensite produced in advance by sub-zero processing. The martensite grows and simultaneously maintains its thin plate when deforming just above M_S temperature. However, when the deforming temperature is higher, it instead grows into a lenticular shape with a different morphology. Furthermore, a well-known general feature of martensitic transformation is the special crystal orientation relationship with the parent austenite phase. For ferrous metals, the martensite crystal orientation relationship with the parent austenite phase is reported to be the Kurdjumov-Sachs (K-S) relationship ($(111)_\gamma$// $(011)_\alpha$, $[\bar{1}01]_\gamma$//$[\bar{1}\bar{1}1]_\alpha$) or the Nishiyama-Wasserman (N-W) relationship ($(111)_\gamma$//$(011)_\alpha$, $[11\bar{2}]_\gamma$//$[01\bar{1}]_\alpha$) [30]. Although few reports exist for deformation-induced martensite, a K-S-like relationship has been confirmed regardless of its formation mechanism[15, 19].

It has been reported that austenite not only improves strength-related properties through the TRIP effect, but also improves the fatigue-related properties of various modes[31-36]. Quenched and tempered steel is used in the bearing rings and rolling elements of rolling bearings. Since the microstructure contains retained austenite along with tempered martensite and cementite, numerous studies have been conducted into the impact of this retained austenite on the rolling contact fatigue (RCF) life[37-50]. These studies report that retained austenite effectively improves RCF life, and may be related to the deformation-induced martensitic transformation of retained austenite as the underlying principle. Other than the suppression of crack propagation like that found in TRIP steel[37], the possibilities of suppressing martensite decomposition[37, 38] and introducing compressive residual stress[39, 40] owing to the generation of new martensite have also been reported. However, this previous work infers the contribution of deformation-induced transformation of retained austenite from measurements of the hardness and residual stress after RCF, and direct observation of deformation-induced martensite is limited. Since studies were mainly conducted using quenched and tempered high carbon chromium bearing steel, the following facts are believed to be the causes of this limitation. For instance, the microstructure was extremely fine, the retained austenite content was low at approximately 10%, and the stresses during rolling contact were complex. Other studies conducted observations of deformation-induced martensites using carburized, quenched, and tempered low carbon steels containing relatively high levels of retained austenite[39, 48]. However, the detailed microstructural character of martensite and its crystal orientation relationship with the parent austenite have not been clarified. The phenomenon of deformation-induced martensitic transformation, which is essential for the improvement of RCF life, has not been directly observed. Compared to the study of high alloy TRIP steels, much remains unclear.

This study intends to clarify both the microstructural character of deformation-induced martensite formed during rolling contact and its formation mechanism. We conducted crystal orientation analysis by electron backscattering diffraction (EBSD) using field emission-scanning electron microscopy (FE-SEM), and automated crystal orientation mapping through nanobeam precession electron diffraction using transmission electron microscopy (ACOM-TEM) to reveal the morphology of deformation-induced martensite and its crystal orientation relationship with the parent austenite.

2. Experimental Methods

2. 1 Specimens

SAE4320 steel was selected as the sample owing to its high Ni content, which is an austenite stabilizer. The chemical composition is shown in **Table 1**. Retained austenite can be easily obtained from SAE4320 steel by carburizing and quenching. A manufactured hot-rolled steel bar of 26mm diameter was cut and subjected to heat treatment, then finished into a cylinder with a diameter of 20mm and width of 36mm by grinding. The heat treatment involved carburizing, quenching, and tempering. For carburization, the specimen was kept for 26 h in a carburizing atmosphere of 960℃ and modified such that the carbon concentration in the surface layer was approximately 1.1%. After soaking for 70 min at 820℃, the specimen was quenched in oil at 80℃, then tempered at 180℃ for 2 h.

Table 1 Chemical composition of steel used (mass%)

C	Si	Mn	P	S	Cu	Ni	Cr	Mo	O
0.20	0.19	0.55	0.018	0.006	0.10	1.70	0.53	0.21	0.0009

2. 2 Rolling Contact Fatigue Test

The machine used for the RCF test is schematically shown in **Fig. 1**. This test machine was used to rotate one specimen against two JIS-SUJ2 steel balls (31.75mm in diameter) supported by three guide rolls. The lubricating

oil was applied to the specimen surface through a driving roll. The test conditions are listed in **Table 2**. The maximum orthogonal shear stress through rolling contact is at a depth of 0.24mm (z_0) from the rolling contact surface. Microstructural change due to RCF is the most prominent at depth z_0 because it is affected by orthogonal shear stress[48]. The test was terminated after 3.7×10^6 cycles, at which point the sample was removed and submitted for microstructural analysis and crystal orientation analysis.

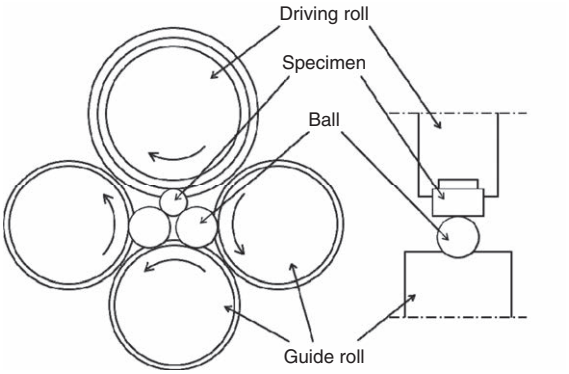

Fig. 1 Schematic of the radial type rolling contact fatigue test machine

Table 2 Rolling contact fatigue test conditions

Contact condition	Herzian maximum pressure	5.8 GPa
	Maximum orthogonal shear stress (depth z_0)	1.4 GPa (0.24mm)
Loading speed		285 Hz
Lubricant		Mineral oil (ISO-VG100)
Operating temperature		60 ± 5℃

2. 3 Microstructural Analysis and Crystal Orientation Analysis

SEM-EBSD measurements of the untested (pre-RCF) and tested (post-RCF) sample were conducted. The specimen for SEM-EBSD was buffed with a 1 μm diamond paste at a section parallel to the rolling contact surface (perpendicular to the ND outlined later), at a depth z_0 from the rolling contact surface, and polished to a mirror finish using colloidal silica. Measurements were taken using an EBSD data collection system (OIM by TSL) attached to an FE-SEM (JSM-7100F by JEOL) at an acceleration voltage 15 kV, a working distance of 15mm and a step size of 40 nm or 10 nm. Grains smaller than the step size cause the Kikuchi pattern to become ill-defined and thereby reduce measuring accuracy. We therefore excluded any low-accuracy data from the data processing sets.

To obtain a more detailed analysis of the post-RCF microstructure, we conducted ACOM-TEM measurements. When the thin film specimen used for this was manufactured using the focused ion beam (FIB) method, we confirmed the transformation of retained austenite during the sample preparation process in advance. Accordingly, we used a precision cutting device to cut a thin film sample with the same cross-section as that of the sample used for SEM-EBSD. To suppress the transformation of retained austenite in the process of producing the thin film specimen, we employed a twin-jet electropolisher using an ethanol/perchloric acid solution (mixed at a volume ratio of 9:1) at a temperature of 10℃. Subsequently, we performed Ar ion milling with a low acceleration voltage to obtain a smooth surface suitable for ACOM-TEM. The equipment used was ASTAR (NanoMEGAS) incorporated in a TEM (JEM-2800 by JEOL). Measurements were taken at an acceleration voltage of 200 kV, a precession angle of 0.5° and a step size of 2 nm.

3. Experimental Results

3. 1 Microstructural Analysis and Crystal Orientation Analysis through SEM-EBSD

To determine the microstructures before and after RCF testing, we analyzed the phase distribution using SEM-EBSD. The measuring range was 16 μm × 32 μm, and step size was 40 nm. **Figure 2** shows the results for the phase map overlaid on the image quality (IQ) map. The rolling, transverse, normal directions (RD, TD, and ND respectively) of the specimen are indicated in **Fig. 2**. Movement of the load (steel ball) during rolling contact is in the opposite direction to the RD. The α phase corresponding to tempered martensite, the γ phase corresponding to retained austenite and cementite can be confirmed in the pre-RCF sample (**Fig. 2**(a)). Subsequently, refinement of the tempered martensite and a reduction in retained austenite in the post-RCF sample can be seen in **Fig. 2**(b), although there is no change in the cementite. This result is the same as previously reported[49]; however, the fine, elongated structure corresponding to white bands (WB) as confirmed in the previous report were not observed because different sections of the material were observed. Moreover, the reduction in retained austenite due to RCF was similar to the that observed by X-ray diffraction in previous research[40, 48, 50, 51]. The X-ray diffraction and SEM-EBSD results suggest the possibility that the deformation-induced transformation of retained austenite into martensite occurs due to rolling contact. However, no corresponding increase in the α phase was observed and thus we cannot conclude that martensite was generated due to the deformation-induced transformation of retained austenite.

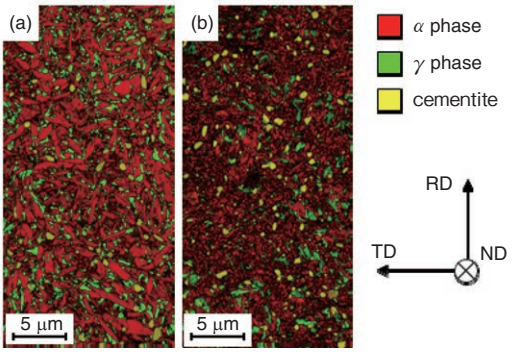

Fig. 2 Phase maps obtained using SEM-EBSD at z_0 depth
(a) Before RCF (b) 3.7×10^6 cycles

The morphology of the martensite generated through the deformation-induced transformation of austenite during rolling contact has been unclear in preexisting literature. It is therefore theorized that martensite exists in an extremely fine form, with no EBSD patterns having been obtained. To observe fine-grained deformation-induced martensites, we therefore conducted EBSD measurements with a step size of 10 nm centering on single retained austenite grains. The pre-RCF IQ + phase map and inverse pole figure (IPF) map are shown in **Fig. 3**. Tempered martensite is present around the retained austenite. Moreover, the grain size of the retained austenite and the tempered martensite is of the order of a few μm. As it consists of high carbon martensite, it is possible that microstructures such as transformation twins are present in the tempered martensite, but this could not be confirmed by the EBSD measurements we conducted. The post-RCF microstructures are shown in **Fig. 4**. Microstructural change due to RCF was confirmed by comparing the results to those in **Fig. 3**. The grain size of the tempered martensite around retained austenite has been refined to submicron proportions due to rolling contact and a variety of crystal orientations were observed. The same results have been obtained in microstructure observations using TEM, and it has been reported that dislocation cells are formed within the tempered martensite through the introduction of plastic strain associated with rolling contact and that fine grains with random orientations are generated[52]. Furthermore, the grain size of the retained austenite remains in the order of a few μm and is not subjected to grain refinement like the tempered martensite. However, the α phase, which was not present prior to RCF and which is even finer than the surrounding tempered martensite, can be observed inside the retained austenite grain. We surmise that this fine α phase is deformation-induced martensite, which was generated from the retained austenite due to rolling contact.

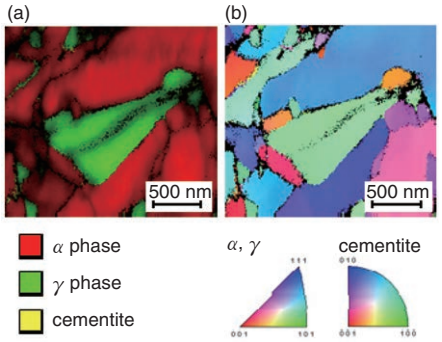

Fig. 3 SEM-EBSD results centered on retained austenite at z_0 depth before RCF
(a) Phase map overlaid on IQ map (b) IPF map

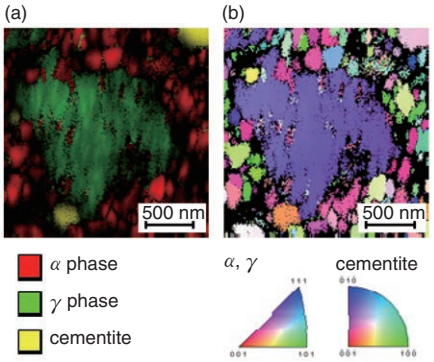

Fig. 4 SEM-EBSD results centered on retained austenite at z_0 depth after RCF
(a) Phase map overlaid on IQ map (b) IPF map

3. 2 Microstructural Analysis and Crystal Orientation Analysis by ACOM-TEM

To further clarify the morphology of deformation-induced martensite, we conducted an ACOM-TEM analysis. To obtain crystal data from the electron diffraction patterns when irradiating a specimen with an electron probe of a few nm, the spatial resolution of ACOM-TEM is one order of magnitude higher than that of SEM-EBSD. In the bright field image in **Fig. 5**(a), a microstructure flatter than the surrounding microstructures was confirmed, which is believed to be a mix of retained austenite and deformation-induced martensite[48]. The phase distribution analysis (**Fig. 5**(b)) shows that the parent phase in the flat microstructure is retained austenite with fine deformation-induced martensites existing inside. Furthermore, the IPF map in **Fig. 5**(c) shows that the retained austenite consists of a single grain with a constant crystal orientation, and that the deformation-induced martensite present inside are individual grains with different crystal orientations. Although it is difficult to quantitatively assess the size of the deformation-induced martensites that were measured with ACOM-TEM, grains smaller than 5 pixels are present and we can

surmise that the smallest measures a few nm. The ACOM-TEM results clearly revealed the presence of extremely fine deformation-induced martensites. In the Discussion section, we will outline the crystal orientation relationship between the retained austenite and deformation-induced martensite, obtained from the SEM-EBSD and ACOM-TEM analysis results.

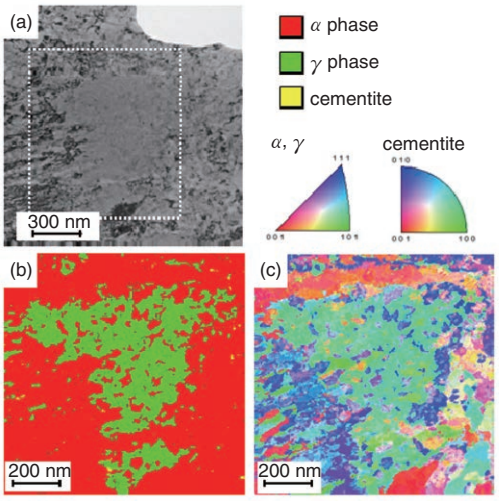

Fig. 5 ACOM-TEM results centered on retained austenite at z_0 depth after RCF.
(a) TEM bright field image (b) Phase map
(c) IPF map
(b)(c) were measured in the white dotted line area of (a)

4. Discussion

4. 1 Crystal Orientation Relationship between Parent Austenite and Deformation-induced Martensite

Martensite is generated with a K-S or N-W crystal orientation relationship with the parent austenite[30]. A K-S relationship has been confirmed for deformation-induced martensitic transformation[15, 19], but no reports exist regarding deformation-induced martensitic transformation during rolling contact, and the details of this phenomenon remain unclear. We therefore studied the crystal orientation relationship between retained austenite and deformation-induced martensite generated during rolling contact. To this end, we extracted the range believed to be a single retained austenite from **Fig. 4** (SEM-EBSD) and **Fig. 5** (ACOM-TEM). Crystals were then rotated so that the γ <001> direction formed the base axis on the stereoprojection and $\{001\}_\alpha$ pole figures were obtained. Results are shown in **Fig. 6**. Although the number of SEM-EBSD measuring points are low, it is clear from **Fig. 6**(c) that multiple variants of the deformation-induced martensites are present. Since there are 24 types in a K-S relationship and 12 types in an N-W relationship, it is believed that several of these variants have occurred. In the ACOM-TEM results (**Fig. 6**(f)), which had many measurement points, variants close to K-S or N-W relationships are presumed to occur as well, although the variation in crystal orientation is large. The accuracy of crystal orientation analysis performed using electron diffraction patterns in ACOM-TEM is lower than that in SEM-EBSD, which uses Kikuchi patterns. Furthermore, since martensite is very fine, diffraction patterns for retained austenite are superimposed, which reduces the accuracy of the analysis. Therefore, it should be considered that the ACOM-TEM results may have a lower crystal orientation accuracy than the SEM-EBSD results. Although SEM-EBSD has few measuring points because very fine deformation-induced martensite was not detected, martensite with K-S or N-W relationships with the parent retained austenite was confirmed, demonstrating that deformation-induced martensite was newly formed during rolling contact. Furthermore, although the accuracy of crystal orientation measurements is not high, similar crystal orientation relationships were confirmed from the ACOM-TEM results, supporting the hypothesis that the nm-sized fine α grains are deformation-induced martensite. The orientational difference between the K-S and N-W relationships was only 5.3°. Therefore, distinguishing between them is difficult under experimental conditions. Since we were also unable to do so in this study, this requires further study and theoretical evidence.

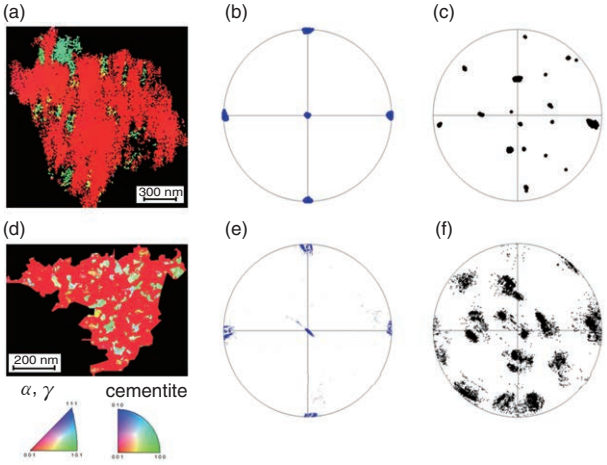

Fig. 6 Crystal orientation relationships between retained austenite and deformation-induced martensites after RCF
(a)-(c) SEM-EBSD analyses (d)-(f) ACOM-TEM analyses
(a)(d) IPF maps (b)(e) $\{001\}_\gamma$ pole figures
(c)(f) $\{001\}_\alpha$ pole figures

4. 2 Mechanism of Deformation-induced Martensitic Transformation

Olson and Cohen[21] demonstrated that if deformation-induced martensite is transformed during the elastic deformation of retained austenite, pre-existing interfaces between tempered martensite and retained austenite (hereinafter referred to as tempered α'/retained γ interface) form the nucleus for stress-induced martensitic transformation. However, if the retained austenite has been subject to plastic deformation, then martensitic transformation occurs from the heterogeneous deformation areas formed inside the retained austenite[21]. The newly formed nuclei of deformation-induced martensite for the latter are surmised to have formed from intersections with shear bands, and it is suggested that this is a strain-induced martensitic transformation. According to Onodera *et al*. [23], Suzuki *et al*. [24], and Ueda and Fujita[25], however, these types of areas are local areas of stress concentration where there is intersection with deformation twins and slip bands. In this case, a type of stress-induced martensitic transformation is expected.

The mechanisms introduced in these previous studies indicate that the deformation-induced martensitic transformation is greatly affected by elastoplastic deformation behavior of the retained austenite. We studied the mechanism of the deformation-induced martensitic formation during rolling contact from the perspective of stress conditions. During rolling contact, principal shear stress is the highest at a particular depth from the rolling contact surface[49]. Using the Herzian contact theory, the principal shear stress at depth z_0, at which we conducted the microstructural analyses, is determined to be approximately 1 807 MPa. Additionally, since no known mean critical resolved shear stress (τ_{CRSS}) is available for austenite in SAE4320 steel or equivalent steels, we used yield stress (σ_Y) of austenite for Fe-Si-Mn-C alloy as reported by Jacques *et al*. [53], who showed that the σ_Y of austenite increases as carbon content increases. σ_Y for austenite with approximately 1.1% carbon content, which corresponds to the retained austenite used in this study, is estimated to be approximately 650 MPa. If τ_{CRSS} (212 MPa) is used as a reference, which was calculated by Eq. (1) using Taylor factor M = 3.07 for fcc polycrystal metals, then the yield criteria for austenite are adequately met, even when considering the stress distribution between the tempered martensite, cementite and their interfaces.

$$\tau_{CRSS} = \sigma_Y / M \quad (1)$$

To facilitate the observation of microstructural change during rolling contact, we conducted RCF testing at higher contact stress settings than those found under regular usage conditions. We also obtained results for the rolling bearing used under standard contact conditions. Using a 6206 deep groove ball bearing (bore diameter 30mm, outside diameter 62mm, width 16mm) as the typical rolling bearing type, we performed the calculations for loading with half the radial load (9.75 kN) of the basic dynamic radial load rating (19.5 kN[54]). Results showed that principal shear stress at depth z_0 was 840 MPa (z_0 = 0.10mm) for the inner ring and 1 041 MPa (z_0 = 0.17mm) for the outer ring, which were both far higher than the austenite τ_{CRSS}. In other words, plastic deformation of the retained austenite is believed to possibly take place for rolling bearings that are used under standard conditions.

Based on the above, we surmise that during rolling contact, plastic deformation of the retained austenite initially occurs followed by the deformation-induced martensitic transformation inside retained austenite grains. In other words, the deformation-induced martensites presumably nucleate in locally formed heterogeneous areas or in the intersecting areas of slip bands, shear bands, and deformation twins. Notably, most deformation-induced martensites appear to have formed inside retained austenite grains (**Fig. 6**(a) and (d)). To obtain a 3D estimation of the generated deformation-induced martensite, we conducted EBSD measurements at the section perpendicular to the TD. Although this retained austenite grain is different from that in **Fig. 4**, analysis was conducted in the same way as shown in **Fig. 6**. Results are shown in **Fig. 7**. **Figure 6**(a) and **Fig. 7**(b), confirm that, regardless of the section measured, deformation-induced martensites are formed inside the retained austenite grains. Based on these observations, we surmise that very fine deformation-induced martensites measuring a few nm in size that are formed inside retained austenite grains due to plastic deformation contribute to improved RCF life.

Unevenness in the shape of the post-RCF tempered α'/retained γ interface is more pronounced than in the pre-RCF interface (**Fig. 3**), as was confirmed by the high spatial resolution ACOM-TEM results (**Fig. 5**(b)). These results suggest the possibility that deformation-induced martensites are formed from the tempered α'/retained γ interface. Olson and Cohen[21] reported that these kinds of grain boundaries potentially formed the nucleus of transformation when austenite had undergone elastic deformation. The mechanism by which deformation-induced martensite present near the tempered α'/retained γ interface is formed will be the focus of our future work.

In the current study we focused on ascertaining the microstructural character of deformation-induced martensite. The systematic analysis of the relationship between the formation of deformation-induced martensite, the deformation behavior of austenite and its deformed structures, along with the study of the 3D shape of deformation-induced martensite inside identical retained

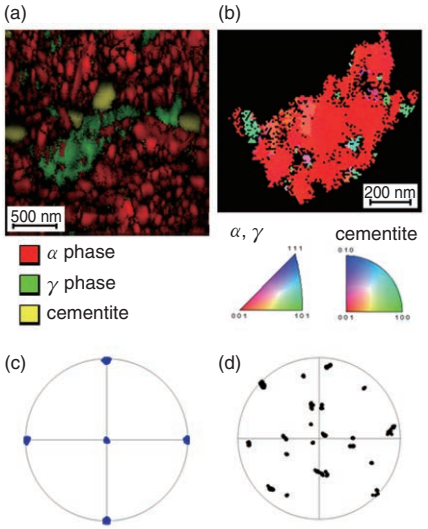

Fig. 7 SEM-EBSD results centered on retained austenite on a section perpendicular to TD at z_0 depth before RCF
(a) Phase map overlaid on IQ map
(b) IPF map of selected single retained austenite grain
(c) $\{001\}_\gamma$ pole figure (d) $\{001\}_\alpha$ pole figure

austenite grains will be the focus of future work. A more complete understanding of the formation and morphology of deformation-induced martensite may be obtained by ascertaining the morphology of deformation-induced martensite through 3D EBSD measurements using serial-sectioning with FIB-SEM. However, as outlined above, surface grinding of microstructures containing retained austenite that is thermally and mechanically unstable due to FIB has many issues for the purpose of microstructural observation, and remains to be investigated in future.

5. Conclusion

After measuring the morphology of deformation-induced martensite generated through rolling contact using SEM-EBSD and ACOM-TEM, we arrived at the following conclusions:

(1) Detailed SEM-EBSD and ACOM-TEM measurements revealed that deformation-induced martensites consist of very fine grains with varying crystal orientations, the smallest of which are only a few nm long. They are formed in various locations but mainly inside retained austenite grains. The crystal orientation relationship between the parent retained austenite and the deformation-induced martensite is similar to K-S or N-W relationships, which is a typical feature of martensitic transformation.

(2) The principal shear stress estimated from the RCF test conducted for this study and the regular usage conditions for rolling bearings is substantially higher than the critical resolved shear stress of retained austenite. Therefore, it is highly likely that plastic deformation of the retained austenite occurs during rolling contact. Accordingly, we surmised that deformation-induced martensites are formed from locally heterogeneous deformation areas or these intersecting areas introduced inside retained austenite grains through plastic deformation.

(3) Future work will aim to define the mechanism of martensitic transformation associated with plastic deformation. Clarification of the transformation mechanism will require the deformed structure which forms the nucleus of the transformation and the 3D microstructures of the deformation-induced martensites to be ascertained. We intend to study this in the future.

References

1) T. ANGEL : Formation of Martensite in Austenitic Stainless Steels, J. Iron Steel Inst., 177 (1954) 165.
2) O. MATSUMURA, Y. SAKUMA and H. TAKECHI: TRIP and its Kinetic Aspects in Austempered 0.4C-1.5Si-0.8Mn Steel, Scr. Metall., Vol. 21, No. 10 (1987) 1301.
3) K. SUGIMOTO, N. USUI, M. KOBAYASHI and S. HASHIMOTO: Effects of Volume Fraction and Stability of Retained Austenite on Ductility of TRIP-aided Dual-phase Steels, ISIJ Int., Vol. 32, No. 12 (1992) 1311.
4) A. ITAMI, M. TAKAHASHI and K. USHIODA: Plastic Stability of Retained Austenite in the Cold-rolled 0.14%C-1.9%Si-1.7%Mn Sheet Steel, ISIJ Int., Vol. 35, No. 9 (1995) 1121.
5) T. NAKAGAITO, H. MATSUDA, Y. NAGATAKI and K. SETO: Effects of Partitioning of Manganese and Silicon during Intercritical Annealing on Transformation Behavior and Mechanical Properties of Low Alloyed TRIP-assisted Steel Sheets, Tetsu-to-Hagané, Vol. 101, No. 8 (2015) 426 (in Japanese).
6) H. NATSUMEDA, A. KITAHARA and S. HASHIMOTO: Effect of Retained Austenite on Mechanical Properties of 5% Mn Steel, Tetsu-to-Hagané, Vol. 102, No. 9 (2016) 525 (in Japanese).
7) K. NOHARA, Y. ONO and N. OHASHI: Composition and Grain Size Dependencies of Strain-induced Martensitic Transformation in Metastable Austenitic Stainless Steels, Tetsu-to-Hagané, Vol. 63, No. 5 (1977) 772 (in Japanese).
8) S. TURTELTAUB and A. S. J. SUIKER: Grain Size Effects in Multiphase Steels Assisted by Transformation-induced Plasticity, Int. J. Solids. Struct., Vol. 43, No. 24 (2006) 7322.

9) A. KISKO, R. D. K. MISRA, J. TALONEN and L. P. KARJALAINEN: The Influence of Grain Size on the Strain-induced Martensite Formation in Tensile Straining of an Austenitic 15Cr-9Mn-Ni-Cu Stainless Steel, Mater. Sci. Eng. A, Vol. 578, (2013) 408.
10) N. S. LIM, H. S. PARK, J. B. SEOL and C. G. PARK: Study of Thermal and Mechanical Stability of Retained Austenite (RA) in TRIP Steels, CAMP-ISIJ, Vol. 29 (2016) 782 (in Japanese).
11) S. FURUKANE and S. TORIZUKA: Effects of Grain Size and Dislocation Density on Strain-Induced Martensitic Transformation in Austenitic Stainless Steels, Tetsu-to-Hagané, Vol. 105, No. 8 (2019) 827 (in Japanese).
12) K. SUGIMOTO, M. MISU, M. KOBAYASHI and H. SHIRASAWA: Effects of Second Phase Morphology on Retained Austenite Morphology and Tensile Properties in a TRIP-aided Dual-phase Steel Sheet, ISIJ Int., Vo. 33, No. 7 (1993) 775.
13) H. MATSUDA, H. NORO, Y. NAGATAKI and Y. HOSOYA: Effect of Retained Austenite Stability on Mechanical Properties of 590 MPa Grade TRIP Sheet Steels, Mater. Sci. Forum, Vol. 638-642 (2010) 3374.
14) W. S. LI, H. Y. GAO, H. NAKASHIMA, S. HATA and W. H. TIAN: In-situ Study of the Deformation-induced Rotation and Transformation of Retained Austenite in a Low-carbon Steel Treated by Quenching and Partitioning Process, Mater. Sci. Eng. A, Vol. 649 (2016) 417.
15) P. YANG, T. Y. LIU, F. Y. LU and L. MENG: Orientation Dependence of Martensitic Transformation in High Mn TRIP/TWIP Steels, Steel Res. Int., Vol. 83, No. 4 (2012) 368.
16) D. DE KNIJF, T. NGUYEN-MINH, R. H. PETROV, L. A. KESTENS and JOHN J. JONAS: Orientation Dependence of the Martensite Transformation in a Quenched and Partitioned Steel Subjected to Uniaxial Tension, J. Appl. Crystallogr., Vol. 47, No. 4 (2014) 1261.
17) J. R. PATEL and M. COHEN: Criterion for the Action of Applied Stress in the Martensitic Transformation, Acta. Metall., Vol. 1, No. 5 (1953) 531.
18) H. C. FIEDLER, B. L. AVERBACH and M. COHEN: The Effect of Deformation on the Martensitic Transformation in Austenitic Stainless Steels, Trans. Am. Soc. Met., Vol. 47 (1955) 267.
19) I. TAMURA, T. MAKI and H. HATO: On the Morphology of Strain-induced Martensite and the Transformation-induced Plasticity in Fe-Ni and Fe-Cr-Ni Alloys, Trans. Iron Steel Inst. Jpn., Vol. 10, No. 3 (1970) 163.
20) T. MAKI, S. SHIMOOKA, M. UMEMOTO and I. TAMURA: The Morphology of Strain-induced Martensite and Thermally Transformed Martensite in Fe-Ni-C Alloys, Trans. Jpn. Inst. Met., Vol. 13, No. 6 (1972) 400.
21) G. B. OLSON and M. COHEN: A Mechanism for the Strain-induced nucleation of Martensitic Transformations, J. Less-Common Met., Vol. 28, No. 1 (1972) 107.
22) A. SATO and M. KATO: Effects of Stress on Phase Transformations and Precipitations, Tetsu-to-Hagané, Vol. 69, No. 14 (1983) 1531 (in Japanese).
23) H. ONODERA, H. OKA and I. TAMURA: A Role of Strain on Deformation-Induced Martensitic Transformation in an Fe-Ni-Cr Alloy, J. Jpn. Inst. Met., Vol. 42, No. 9 (1978) 898 (in Japanese).
24) T. SUZUKI, H. KOJIMA, K. SUZUKI, T. HASHIMOTO and M. ICHIHARA: An Experimental Study of the Martensite Nucleation and Growth in 18/8 Stainless Steel, Acta. Metall., Vol. 25, No. 10 (1977) 1151.
25) S. UEDA and H. FUJITA: Strain-Induced FCC(γ)→BCC(α') Transformation and Active Slip Systems in Fe-Cr-Ni Alloys, J. Jpn. Inst. Met., Vol. 41, No. 10 (1977) 1007 (in Japanese).
26) V. F. ZACKAY, E. R. PARKER, D. FAHR and R. BUSCH: The Enhancement of Ductility in High-strength Steels, Trans. Am. Soc. Met., Vol. 60 (1967) 252.
27) G. B. OLSON and M. COHEN: Kinetics of Strain-induced Martensitic nucleation, Metall. Trans. A, Vol. 6 (1975) 791.
28) T. KATAYAMA and H. FUJITA: Formation Process of Strain-Induced $\gamma \rightarrow \alpha$' Martensitic Transformation Through the ε Phase, J. Jpn. Inst. Met., Vol. 52, No. 10 (1988) 935 (in Japanese).
29) A. SHIBATA, T. MURAKAMI, S. MORITO, T. FURUHARA and T. MAKI: The Origin of Midrib in Lenticular Martensite, Mater. Trans., Vol. 49, No. 6 (2008) 1242.
30) G. MIYAMOTO, N. TAKAYAMA and T. FURUHARA: Accurate Measurement of the Orientation Relationship of Lath Martensite and Bainite by Electron Backscatter Diffraction Analysis, Scr. Mater., Vol. 60, No. 12 (2009) 1113.
31) T. FURUKAWA, S. KONUMA and S. NISHIWAKI: Effects of Microstructure and Carbon Content in the Case on the Fatigue Strength Properties of Carburized Steel, Tetsu-to-Hagané, Vol. 67, No. 3 (1981) 596 (in Japanese).
32) R. H. RICHMAN and R. W. LANDGRAF: Some Effects of Retained Austenite on the Fatigue Resistance of Carburized Steel, Metall. Trans. A, Vol. 6 (1975) 955.
33) R. J. JOHNSON: Metals Eng. Q., Vol. 15 (1975) 1.

34) B. A. SHAW, F. B. ABUDAIA and J. T. EVANS: Characterization of Retained Austenite in Case Carburized Gears and its Influence on Fatigue Performance, Proc. 20th Conf. of Heat Treating, ASM International, Materials Park, OH, (2001) 62.
35) D. JEDDI and H.-P. LIEURADE: Effect of Retained Austenite on High Cycle Fatigue Behavior of Carburized 14NiCr11 Steel, Procedia Eng., Vol. 2, No. 1 (2010) 1927.
36) T. OGAWA, M. KOYAMA, Y. NISHIKURA, K. TSUZAKI and H. NOGUCHI: Fatigue Behavior of Fe-Cr-Ni-based Metastable Austenitic Steels with an Identical Tensile Strength and Different Solute Carbon Contents, ISIJ Int., Vol. 58, No. 10 (2018) 1910.
37) E. YAJIMA, T. MIYAZAKI, T. SUGIYAMA and H. TERAJIMA: Effect of Retained Austenite on the Rolling Fatigue Life of Ball Bearing Steels, Trans. Jpn. Inst. Met., Vol. 15, No. 3 (1974) 173.
38) A. SHIKO, K. OKAMOTO and S. WATANABE: Effects of Metallographical Factors on the Rolling Fatigue Life of Ball Bearing Steel, Tetsu-to-Hagané, Vol. 54, No. 13 (1968) 1353 (in Japanese).
39) D. ZHU, F. X. WANG, Q. G. CAI, M. X. ZHENG and Y. Q. CHENG: Effect of Retained Austenite on Rolling Element Fatigue and its Mechanism, Wear, Vol. 105, No. 3 (1985) 223.
40) R. C. DOMMARCO, K. J. KOZACZEK, P. C. BASTIAS, G. T. HAHN and C. A. RUBIN: Residual Stresses and Retained Austenite Evolution in SAE52100 Steel under Non-ideal Rolling Contact Loading, Wear, Vol. 257, No. 11 (2004) 1081.
41) T. FUKUI, K. MATUDA and T. TOKUNAGA: Influence of Work Hardening on the Rolling Contact Fatigue Strength of Austenitic Stainless Steel (SUS304), J. Soc. Mater. Sci. Jpn., Vol. 33, No. 371 (1984) 1033 (in Japanese).
42) S. SHOJI and T. EGUCHI: Hadayakikou no Tendouhiroujumyou nioyobosu Zanryuosutenaito no Eikyou, Tetsu-to-Hagané, Vol. 73, No. 5 (1987) S464 (in Japanese).
43) N. TSUSHIMA: Improvement of Rolling Contact Fatigue Life of Bearing Steels, Bull. Jpn. Inst. Met., Vol. 23, No. 1 (1984) 50 (in Japanese).
44) H. MURO, Y. SADAOKA, S. ITO and N. TSUSHIMA: The Effect of Retained Austenite on the Rolling Contact Fatigue of Carburized Steels, Proc. 12th Japan Congr. on Materials Research-Metallic Materials, The Society of Materials Science, Japan, Kyoto, (1969) 74 (in Japanese).
45) T. YAMAMOTO: Jikuukekou no Shinpo to Genjou, Bull. Jpn. Inst. Met., Vol. 11, No. 6 (1972) 419 (in Japanese).
46) N. TSUSHIMA and K. MAEDA: Influence of Retained Austenite on Rolling Contact Fatigue Strength and Wear Strength, Netsu Shori (J. Jpn. Soc. Heat Treat.), Vol. 32, No. 1 (1992) 43 (in Japanese).
47) D. SCOTT and J. BLACKWELL: The Effect of some Manufacturing Variables on the Performance of High-speed Tool-steel Ball Bearings, Wear, Vol. 18, No. 1 (1971) 19.
48) K. KANETANI, T. MIKAMI and K. USHIODA: Effect of Retained Austenite on Sub-surface Initiated Spalling during Rolling Contact Fatigue in Carburized SAE4320 Steel, ISIJ Int., Vol. 60, No. 8 (2020) 1774.
49) K. KANETANI and K. USHIODA: Mechanism of White Band (WB) Formation due to Rolling Contact Fatigue in Carburized SAE4320 Steel, Mater. Trans., Vol. 61, No. 9 (2020) 1750.
50) M. HISHIKI, T. HORI, H. KOHNO, H. KAWABE and M. UEMURA: The Effect of Retained Austenite upon the Life of Steel Balls, J. Jpn. Soc. Precis. Eng., Vol. 44, No. 527 (1978) 1321 (in Japanese).
51) T. FUJITA, K. OGI, T. FUKUI and M. SUENAGA: Influences of Retained Austenite on Rolling Contact Fatigue Strength of Austempered Spheroidal Graphite Cast Iron, Imono (J. Jpn. Foundarymen's Soc.), Vol. 63, No. 9 (1991) 775 (in Japanese).
52) N. MITAMURA, H. HIDAKA and S. TAKAKI: Microstructural Development in Bearing Steel during Rolling Contact Fatigue, Mater. Sci. Forum, Vol. 539-543 (2007) 4255.
53) P. J. JACQUES, Q. FURNEMONT, S. GODET, T. PARDOEN, K. T. CONLON and F. DELANNAY: Micromechanical Characterisation of TRIP-assisted Multiphase Steels by in situ Neutron Diffraction, Philos. Mag., Vol. 86, No. 16 (2006) 2371.
54) ISO 281 : 2007, Rolling bearings – Dynamic load ratings and ratings life.



K. KANETANI* T. MORONAGA** T. HARA***

K. USHIODA****

* *Material R&D Dept., Research & Development Headquarters, Doctor of Engineering*
** *Electron Microscopy Analysis Station, National Institute for Materials Science*
*** *Electron Microscopy Analysis Station, National Institute for Materials Science, Doctor of Engineering*
**** *Division of Mechanical Science and Engineering, Graduate School of Natural Science and Technology, Kanazawa University, Doctor of Engineering*